arXiv:2511.08292v1 [q-bio.NC] 11 Nov 2025

Distance by de-correlation: Computing distance with heterogeneous grid cells

Pritipriya Dasbehera[1, 6], Akshunna S. Dogra[2, 3, 4, 6], and William T. Redman[5, 6, *]

[1]School of Physical Sciences, National Institute of Science Education and Research, India
[2]Center for Doctoral Training in Mathematics of Random Systems: Analysis, Modelling and Algorithms, Imperial College London and Oxford University, UK
[3]Department of Mathematics, Imperial College London, UK
[4]NSF AI Institute for Artificial Intelligence and Fundamental Interactions, USA
[5]Department of Electrical and Computer Engineering, Johns Hopkins University, USA
[6]MathePhysics, India
[*]Correspondence: wredman4@jh.edu

November 12, 2025

Abstract

Encoding the distance between locations in space is essential for accurate navigation. Grid cells, a functional class of neurons in medial entorhinal cortex, are believed to support this computation. However, existing theories of how populations of grid cells code distance rely on complex coding schemes, with assumptions that may not be met by anatomical constraints. Inspired by recent work finding grid cells to have small, but robust heterogeneity in their grid properties, we hypothesize that distance coding can be achieved by a simple de-correlation of population activity. We develop a mathematical theory for describing this de-correlation in one-dimension, showing that its predictions are consistent with simulations of noisy grid cells. Our simulations highlight a non-intuitive prediction of such a distance by de-correlation framework. Namely, that some further distances are better encoded than some nearer distances. We find evidence of this "sweet spot" in previously published rodent behavioral experiments and demonstrate that a decoder which estimates distance from the de-correlation of populations of simulated noisy grid cells leads to a similar pattern of errors. Finally, by simulating noisy grid cells in two-dimensions, we find that there exists a trade-off between the range of distances that can be encoded by de-correlation of population activity and the distinguishability of different distances, which is controlled by the amount of variability in grid properties. We show that the previously observed average amount of grid property variability strikes a balance between the two, enabling the encoding of distances up to several meters. Our work provides new insight on how grid cells can underlie the coding of distance, without the assumptions previously needed, and why grid cells may have small amounts of heterogeneity in their grid properties.

1 Introduction

Grid cells, which are a functional class of neurons found in medial entorhinal cortex (MEC) [1, 2], are canonically viewed as providing a metric for space, encoding the distance between points [3–5] and enabling spatial navigation [6, 7]. This presumed computational role is supported by experimental work showing that distortions in grid firing patterns are correlated with errors in distance estimation [8]. Furthermore, lesioning or inhibiting MEC leads to a significant increase in distance estimation error [9, 10].

Theoretical work and analysis of neurophysiological data have shown that, up to the distance of half a grid spacing (of order 1 m), distance can be decoded from grid cells through their population activity

(referred to as the "population vector") [5, 11, 12]. In particular, the greater the distance between two points, the larger the distance between corresponding population vectors. This demonstrates that, on a limited spatial scale, grid cells provide a conformal isometry [13]. To encode distances beyond half a grid spacing, which is necessary for spatial navigation of real-world environments, a more complex neural code has been hypothesized [3]. In particular, the quasi-periodic relationship between the firing fields of grid cells from different grid modules, which differ in their intrinsic grid spacing and orientation [2], generates a code with high capacity [3, 14]. This code has been shown to be robust to noise [14], but how downstream brain regions can extract this information, especially when they receive inputs from a minority of the grid modules [15], is unclear.

Recent work has shown that individual grid modules contain grid cells with not a single grid spacing and orientation, as has often been assumed in theoretical analysis, but small, yet robust variability in their grid properties [16]. This heterogeneity in grid spacing and orientation was shown to enable *single* grid modules to encode local spatial information [16], a computation which previously had been thought to require the integration of activity from multiple grid modules [17–19]. However, to achieve a high level of accuracy, simulations showed that hundreds of grid cells were needed. Furthermore, decoding spatial position from grid cell activity coming from just two grid modules led to significantly better accuracy, with a lower requirement on population size [16]. It has also been shown that non-grid cells in the MEC can contain robust firing patterns [20], which could be leveraged to further improve decoding accuracy of spatial position [21]. These results question whether a code that leverages variability in grid properties is used by the brain to encode local spatial information. A natural question that then emerges is, are there any other benefits grid property heterogeneity could confer to the grid code? And if so, could any of these provide advantages over integrating activity across multiple grid modules?

Motivated by the putative role of grid cells for distance coding, we hypothesize that grid property variability could enable a simple and efficient to achieve this (Fig. 1). In particular, if there is no variability in grid properties (Fig. 1A), then the correlation of the population vector, at any distance that is an integer multiple of the grid spacing, with the population vector at some reference location ($x = 0$) is constant (Fig. 1D). This is due to the degeneracy in grid firing fields, as every grid cell in the module is the same, up to a translation. When activity from grid cells across multiple modules, each without any variability in grid properties, is considered (Fig. 1B), a symmetry breaking occurs, and the population vector, at integer multiples of the grid spacing, has a unique correlation with the population vector at $x = 0$ (Fig. 1E). However, because of the quasi-periodic relationship between different grid modules, there is not a monotonic relationship between distance and correlation. With this coding scheme, a smaller correlation *does not* imply a greater distance. This can make it challenging to decode distance in a simple way. But, when grid cell activity from a single grid module with non-zero variability in grid properties is considered, not only is there again a symmetry breaking (Fig. 1C), but population vectors at integer multiples of the grid spacing have correlations with the population vector at $x = 0$ that monotonically decay with distance (Fig. 1F). Thus, in this case, a smaller correlation *does* imply a greater distance.

Here, we examine the hypothesis of grid cells enabling a "distance by de-correlation" coding scheme in detail. First, we develop a theory for how variability in grid properties affects the population vector correlation of grid cells, as a function of distance, in one-dimensional (1D) environments (Sec. 2.1). We provide numerical support for the validity of this theory through the simulation of noisy synthetic grid cells. Next, we highlight the fact that the simulations make a prediction that the fidelity with which populations of heterogeneous grid cells encode distance should decrease, then increase, and then decrease again (Sec. 2.2). We find experimental support of this "sweet spot" in prior work that trained mice to travel specific distances [10]. Furthermore, we show that decoding distance from simulated grid cells produces similar results to what was found experimentally. Finally, we perform numerical simulations in two-dimensional (2D) spaces (Fig. 2.3). We find that, as in the 1D case, there exists a trade-off between the fidelity with which distances can be encoded through de-correlation and the total distance over which the de-correlation occurs. This trade-off is controlled by the amount of variability in grid properties, and simulating many combinations allows us to identify that the average heterogeneity in grid spacing and orientation identified

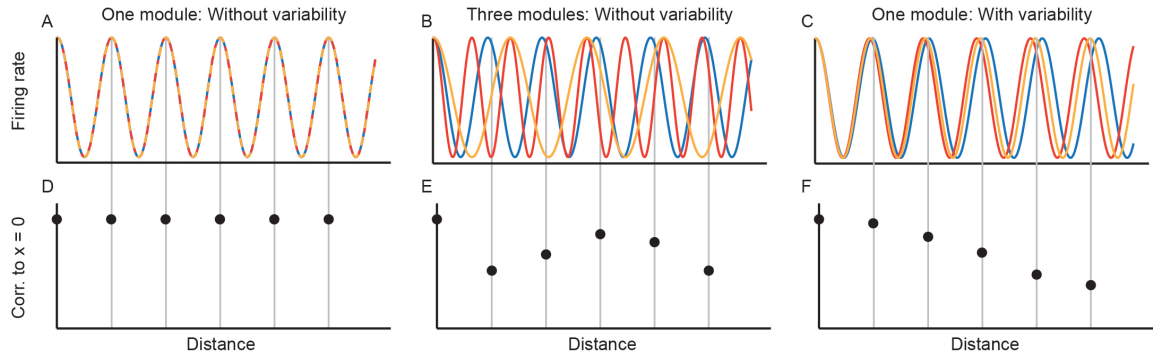

Figure 1: **Schematic of how variability in grid spacing may lead to monotonic relationship between distance and population vector correlation.** (A)–(C) Example idealized 1D firing fields for grid cells coming from: one module, with no variability in grid spacing (A); three modules with no variability in grid spacing (B); and one module with variability in grid spacing (C). (D)–(F) Example correlation between population vectors, corresponding to distances of integer multiples of the grid spacing, with the population vector corresponding to the starting location, for the same populations of grid cells as (A)–(C).

previously [16] strikes a balance between the two ends of the trade-off.

Collectively, our results demonstrate that small heterogeneity in grid properties enables a simple decoding scheme of distance, providing a more plausible mechanism by which grid cells may contribute to distance coding than has been considered previously.

2 Results

2.1 Grid property variability and distance coding in 1D

We begin by developing a theory for how heterogeneity in grid properties affects the population level autocorrelation function. To make the analysis tractable, we consider a 1D environment.

We model grid cell activity as a sum of Gaussians, each centered along integer multiples of the grid spacing,

$$G_{\lambda,\omega}(x) = \sum_{n\in\mathbb{Z}} \exp\left(\frac{-(x-n\lambda)^2}{2\omega^2}\right), \tag{1}$$

where λ is the grid spacing and ω is the width of the Gaussian. In addition to grid spacing, grid cells are described by their grid orientation, θ, and their grid phase, ϕ (e.g., the translation along the $x-$axis of the grid fields). We further simplify by assuming $\theta = 0°$ and $\phi = 0$ m. This is consistent with some experimental work showing a locking of grid fields to the starting location in 1D environments [22].

Eq. 1 is equivalent to a convolution of a Dirac comb with a Gaussian,

$$G_{\lambda,\omega}(x) = \mathrm{comb}_\lambda(x) * g_\omega(x), \tag{2}$$

where $g_\omega(x) = \exp(-x^2/2\omega^2)$ and $*$ is the convolution operator. In this form, the Fourier transform becomes,

$$\widehat{G}_{\lambda,\omega}(\xi) = \widehat{\mathrm{comb}}_\lambda(\xi) \cdot \widehat{g}_\omega(\xi). \tag{3}$$

Eq. 3 can be further realized as

$$\widehat{G}_{\lambda,\omega}(\xi) \propto \sum_{k\in\mathbb{Z}} \delta\left(\xi - \frac{2\pi k}{\lambda}\right) \cdot e^{-\frac{1}{2}\omega^2\xi^2}, \tag{4}$$

where $\delta(\cdot)$ is the Dirac delta operator. The power spectrum of $\widehat{G}_{\lambda,\omega}(\xi)$ is therefore given by

$$\left|\widehat{G}_{\lambda,\omega}(\xi)\right|^2 \propto \sum_{k\in\mathbb{Z}} \delta\left(\xi - \frac{2\pi k}{\lambda}\right) \cdot e^{-\omega^2\xi^2}. \tag{5}$$

By the Wiener–Khinchin theorem, the autocorrelation, $R_{\lambda,\omega}(r)$, is the inverse Fourier transform of the power spectrum [23]. In real space, one convenient representation is

$$R_{\lambda,\omega}(r) \propto \mathrm{comb}_\lambda(r) * e^{-r^2/(4\omega^2)} = \sum_{n\in\mathbb{Z}} e^{-\frac{(r-n\lambda)^2}{4\omega^2}}. \tag{6}$$

That is, the autocorrelation is a sum of Gaussians, each with width $\sqrt{2}\omega$. This is in agreement to the fact that autocorrelation of a Gaussian with width ω is another Gaussian of width $\sqrt{2}\omega$.

We now consider a population of N grid cells, each with their own grid spacing, λ. We denote the collection of spacings by $\Lambda = \{\lambda_i\}_{i=1}^N$. We will assume that they all have a fixed width, ω. We can consider the average population activity as

$$G_{\Lambda,\omega}(x) = \frac{1}{N}\sum_{i=1}^{N} G_{\lambda_i,\omega}. \tag{7}$$

If each λ_i is sampled from a distribution, $\mathcal{D}$, then we can consider the ensemble averaged (or expected) value, $\mathbb{E}_{\mathcal{D}}[G_{\Lambda,\omega}(x)]$. As the Fourier transform is a linear operation, we can take the expectation on $\widehat{G}_{\Lambda,\omega}(\xi)$.

From the above formulation, we can see that a lack of variability in grid spacing (i.e., $\lambda_i = \lambda$), which is assumed in the "traditional" perspective on grid cells, leads the population average activity (Eq. 7) to be the same as a single grid cell (as all grid cells are the same). Therefore, the autocorrelation (Eq. 6) exhibits periodicity that does not decay (Fig. 1A, D) and cannot be used for encoding information about distance. However, if we consider a population of grid cells with variability in grid spacing (like was found in neurophysiological recordings [16]), and we assume that $\lambda_i \sim \mathcal{N}(\lambda, \sigma_\lambda^2)$, then the harmonic frequencies of the Fourier transform, $\xi_k(\lambda) = 2\pi k/\lambda$, get shifted. For small variability ($\sigma_\lambda << \lambda$), a first-order Taylor series expansion gives

$$\xi_k(\lambda_i) \approx \xi_k(\lambda) + \frac{d\xi_k}{d\lambda}\Big|_\lambda (\lambda_i - \lambda), \tag{8}$$

where $d\xi_k/d\lambda = -2\pi k/\lambda^2$.

Hence, to leading order,

$$\xi_k(\lambda_i) \sim \mathcal{N}\left(\mu_k, \sigma_k^2\right), \tag{9}$$

where $\mu_k = 2\pi k/\lambda$ and $\sigma_k = 2\pi|k|\sigma_\lambda/\lambda^2$. Thus, each spectral line at $\xi_k(\lambda)$ becomes broadened into a Gaussian of width σ_k. Averaging over the distribution of λ_i therefore yields

$$\mathbb{E}_{\lambda_i}\left[\widehat{G}_{\lambda,\omega}(\xi)\right] \propto \sum_{k\in\mathbb{Z}} \exp\left(\frac{-(\xi-\mu_k)^2}{2\sigma_k^2}\right) \cdot e^{-\frac{1}{2}\omega^2\xi^2}. \tag{10}$$

The expected power distribution, in the limit of $\sigma_k << 1$, becomes

$$\left|\mathbb{E}_{\lambda_i}\left[\widehat{G}_{\lambda,\omega}(\xi)\right]\right|^2 \propto \sum_{k\in\mathbb{Z}} \exp\left(\frac{-(\xi-\mu_k)^2}{2\sigma_k^2}\right)^2 \cdot e^{-\omega^2\xi^2} \approx \sum_{k\in\mathbb{Z}} \exp\left(\frac{-(\xi-\mu_k)^2}{\sigma_k^2}\right) \cdot e^{-\omega^2\xi^2}. \tag{11}$$

From Eq. 11, we see that our theory makes several predictions on the expected power distribution, and hence, on the expected autocorrelation of the activity of population of grid cells with variable grid spacing. In particular, we note that since $\sigma_k = 2\pi|k|\sigma_\lambda/\lambda^2$, Eq. 11 predicts that $\left|\mathbb{E}_{\lambda_i}\left[\widehat{G}_{\lambda,\omega}(\xi)\right]\right|^2$ will:

- (**P1**) Smoothly decay with increased distance, as $\sigma_k \propto k$;
- (**P2**) Exhibit an increased rate of decay with increased variability in spacing, as $\sigma_k \propto \sigma_\lambda$;
- (**P3**) Exhibit a decreased rate of decay with increased grid spacing, since $\sigma_k \propto \frac{1}{\lambda^2}$.

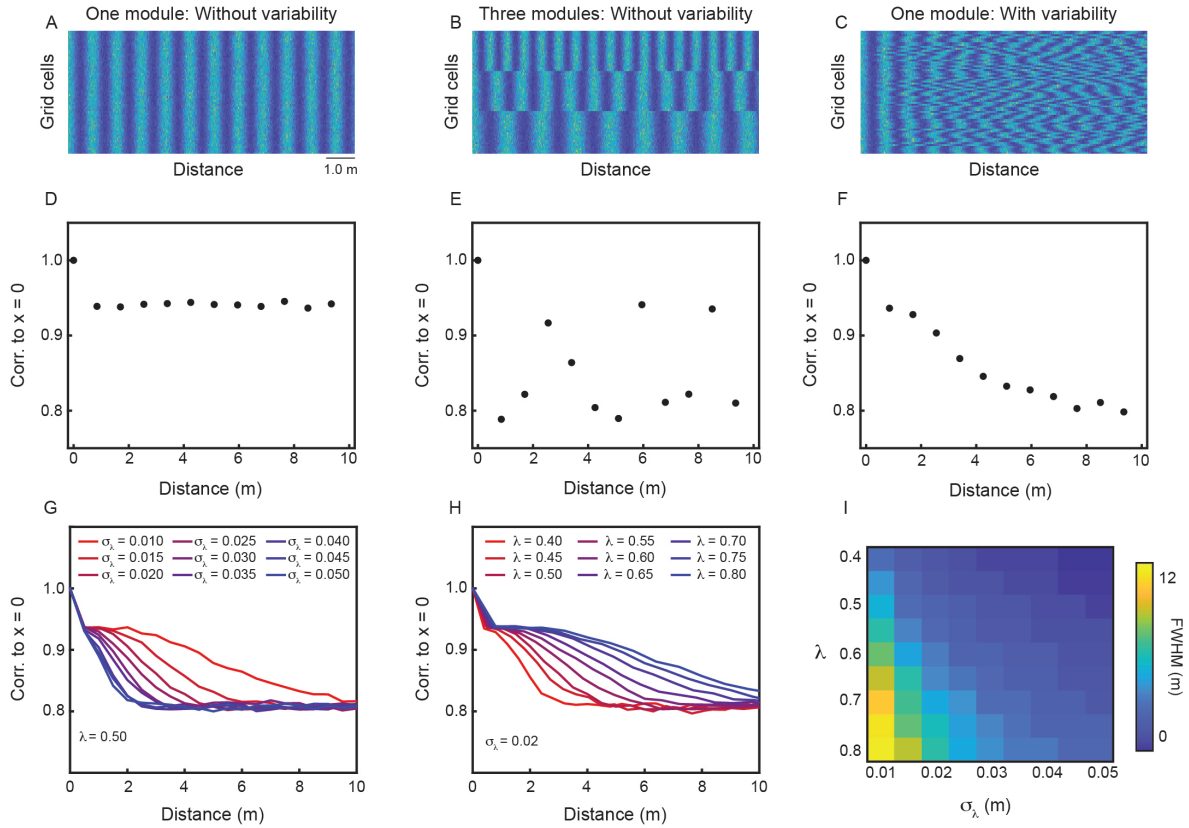

Figure 2: **Variability in grid spacing leads to monotonic relationship between population vector correlation and distance in 1D.** (A)–(C) Noisy synthetic grid cell ratemaps in 1D for populations comprising of: a single module with no variability in grid spacing (A) ($\lambda = 0.85$ m and $\sigma_\lambda = 0$ m); three modules with no variability in grid spacing (B) ($\lambda_1 = 0.60$ m, $\lambda_2 = 0.85$ m, $\lambda_3 = 1.20$ m, and $\sigma_{\lambda_m} = 0$ m); and one module with variability in grid spacing (C) ($\lambda = 0.85$ m and $\sigma_\lambda = 0.05$ m). For all populations, the grid orientation is set to 0° and the phase of all grid cells is set to 0 m. (D)–(F) Correlation of population vectors, corresponding to distances of integer multiples of the grid spacing, with the population vector corresponding to the starting location, for the same populations of grid cells as (A)–(C). (G) Population vector correlation, as a function of distance, for different grid spacing variabilities, σ_λ. λ is fixed at 0.5 m. (H) Population vector correlation, as a function of distance, for different grid spacings, λ. σ_λ is fixed at 0.02 m. (I) The full width at half maximum (FWHM) of the population vector correlation curves, for different combinations of λ and σ_λ. For all plots, $N = 64$ and 25 distinct populations were simulated.

We test these predictions by simulating populations of noisy synthetic grid cells and examining the population vector correlation along increasing integer multiples of the grid spacing. In particular, we sample idealized grid cell ratemaps, constructed using standard approaches [24], and use them as the means of a Poisson process (see Appendix A, for more details).

We simulate three types of grid cell populations: grid cells coming from a single module with no variability in grid spacing ($\sigma_\lambda = 0$ m) (Fig. 2A); grid cells coming from three modules, each having their own spacing – λ_m, which are related by $\lambda_{m+1} = \sqrt{2}\lambda_m$, which is consistent with previous experimental findings [2] – and having no variability in grid spacing ($\sigma_{\lambda_m} = 0$ m) (Fig. 2B); grid cells coming from a single module with variability in grid spacing ($\sigma_\lambda = 0.05$ m) (Fig. 2C). Consistent with **P1**, we find that the population vector correlation smoothly decays as a function of distance for the population of grid cells with non-zero σ_λ (Fig. 2F). This is not observed for the other two populations (Fig. 2D, E), demonstrating that this is a property unique to grid cell populations with heterogeneous grid spacing.

We then fix λ and vary σ_λ. Consistent with **P2**, we find that increasing σ_λ leads to an accelerated decay in the population vector correlation (Fig. 2G). For instance, when $\sigma_\lambda = 0.01$ m, the population vector correlation does not decay to its baseline until almost 10 m, exhibiting near monotonic decrease in

correlation from 2 m to 10 m. In contrast, when $\sigma_\lambda = 0.04$ m, the population vector correlation decays to baseline by 2 m.

When we fix σ_λ and vary λ, we find that increasing λ leads to slower decay of population vector correlation (Fig. 2H), in-line with **P3**. Simulating a wide range of pairs of λ and σ_λ, we find that **P2** and **P3** are robustly supported (Fig. 2I), demonstrating that our simplified theory can provide insight that is consistent with noisy populations of grid cells.

2.2 Existence of sweet spot in distance coding in 1D

The population vector correlation as a function of distance curves computed through our numerical simulations demonstrate that, after the initial decrease in correlation when moving from the starting location ($x = 0$) to the first grid spacing ($x = \lambda$), the correlation has an approximately sigmoidal dependence on distance (Fig. 2G, H). As a consequence of this, the difference in correlation between neighboring points is not uniform. More precisely, if the population vector correlation function has a sigmoidal form

$$C(x) \propto \frac{1}{1 + e^{-\beta(x-\nu)}}, \tag{12}$$

then the derivative of the correlation function is

$$\frac{dC(x)}{dx} \propto \frac{-\beta e^{-\beta(x-\nu)}}{\left[1 + e^{-\beta(x-\nu)}\right]^2}, \tag{13}$$

where β controls the slope of the sigmoid, ν determines the midpoint of the sigmoid, and $x = n\lambda$, $n \in \mathbb{N}$. From Eq. 13, we see that the maximum value of $dC(x)/dx$ is $\beta/4$, which occurs at $x = \nu$. This predicts that there exists a "sweet spot", where the difference in correlation between neighboring integer multiples of the grid spacing is maximal and thus, the distinguishability of distance based on correlation is increased.

To test this prediction, we first measure the finite difference in correlation (DoC) of the simulated $C(x)$ curves (Fig. 3A). That is,

$$\mathrm{DoC}(n\lambda) = \frac{1}{2}\Big(\big|C[n\lambda] - C[(n-1)\lambda]\big| + \big|C[n\lambda] - C[(n+1)\lambda]\big|\Big). \tag{14}$$

As predicted by Eq. 13, we find that the DoC has a peak (Fig. 3B, C – triangles), whose magnitude and location varies with the slope and midpoint of the correlation function (compare Fig. 3B, C with Fig. 2G, H). Looking across different combinations of λ and σ_λ, we find a trade-off between the maximum value of the DoC (Fig. 3D) and the distance at which the maximum is realized (Fig. 3E).

The existence of a sweet spot provides a non-intuitive prediction that the accuracy in decoding distance from grid cell activity should be non-monotonic. That is, the error should increase, then decrease, then increase again. Remarkably, we find evidence for this in previous rodent behavioral experiments. Tennant et al. (2018) trained mice to run along a 1D virtual environment and stop at specific distances, within a 0.2 m zone, to get a reward [10]. These distances ranged from 0.88 m to 4.81 m. In the case where there was a visual stimulus that marked the start of the reward zone (referred to as "beaconed" trials), the mice performed with high accuracy (Fig. 4A – blue triangles). On trials where there was no visual stimulus and the mice had to rely solely on an internal sense of how far they had traveled (referred to as "probe" trials), they performed with moderate accuracy, on average stopping short of the reward zone (Fig. 4A – red squares). Analyzing the publicly available data, we find that the absolute error in the stopped location, with respect to the true reward location, was non-monotonic, increasing when the reward zone location was at 2.3 m, decreasing when the reward zone was at 3.3 m, and then increasing again when the reward zone was at 4.8 m (Fig. 4B). This decrease in absolute error at 3.3 m is particularly striking, given that the total distance traveled by the animal increased relative to when the reward location was at 2.3 m.

To further demonstrate that the behavioral data collected by Tennant et al. (2018) is consistent with a distance coding scheme that leverages heterogeneity in grid properties, we perform a decoding analysis on

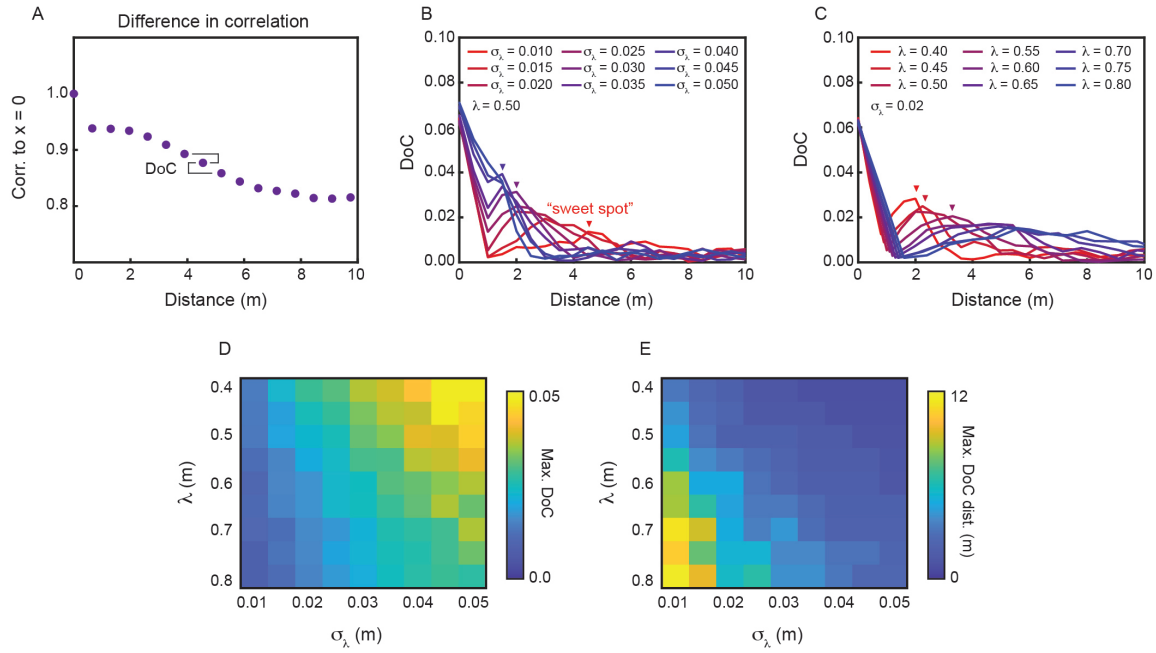

Figure 3: **Grid spacing and grid spacing variability control trade-off between range over which decorrelation occurs and distinguishability between neighboring distances.** (A) Schematic illustration of the difference of correlation (DoC) for one example distance. (B) DoC, as a function of distance, for different grid spacing variabilities, σ_λ. λ is fixed at 0.5 m. (C) DoC, as a function of distance, for different grid spacings, λ. σ_λ is fixed at 0.02 m. (D) Maximum DoC value for different combinations of λ and σ_λ. (E) Distance at which the maximum DoC value occurs, for different combinations of λ and σ_λ. For all plots, $N = 128$ and 25 unique populations were simulated.

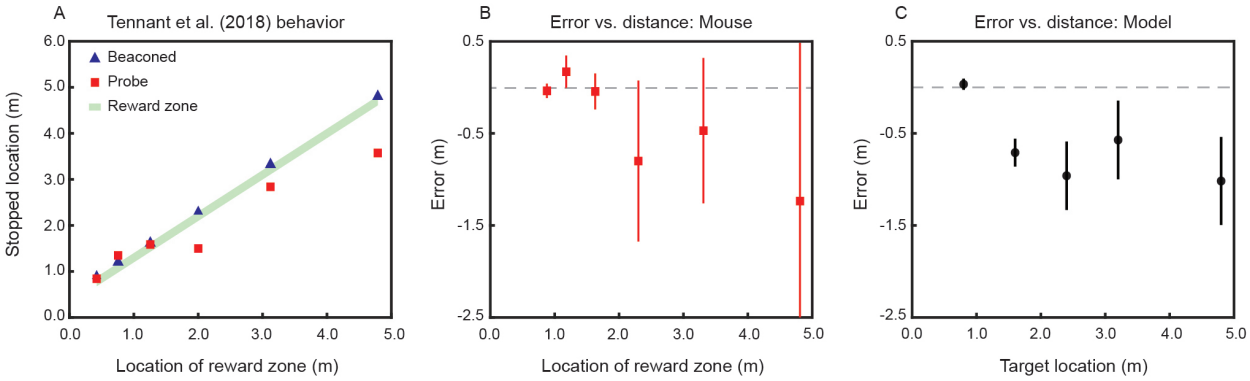

Figure 4: **Sweet spot distance coding is seen in experimental data and simulations of heterogeneous grid cell populations.** (A) Average stopped location of mice on beaconed and probed trials from Tennant et al.'s (2018) behavioral experiments [10]. Subpanel is analogous to their Fig. 3D. (B) Error in stopped location, with respect to the true location of the reward zone of mice, from Tennant et al.'s (2018) behavioral experiments. Error bars are $\pm$ standard deviation across $4-7$ mice (number of animals differs across each distance). (C) Error in decoded location, with respect to target location, from noisy synthetic grid cell populations. $\lambda = 0.80$ m, $\sigma_\lambda = 0.05$ m, and $N = 64$. Error bars are $\pm$ standard deviation across 7 uniquely sampled populations.

simulated noisy grid cell populations (see Appendix B, for more details). We find that, if we set $\lambda = 0.8$ m and $\sigma_\lambda = 0.05$ m, a similar trend to that observed in the Tennant et al. (2018) emerges (compare Fig. 4C with Fig. 4B). The decoding error is approximately 0.0 m when the "target location" is at the first grid spacing ($x = 1 \cdot \lambda = 0.8$ m). When the target location is at three grid spacings ($x = 3 \cdot \lambda = 2.4$ m), the decoding error is around -1.0 m. When the target location is increased to four grid spacings ($x = 4 \cdot \lambda = 3.2$ m), the decoding error improves to approximately -0.5 m. And by six grid spacings ($x = 6 \cdot \lambda = 4.8$ m), the decoding error becomes nearly -1.5 m. This general consistency with experimental findings supports our hypothesis that grid cells with variable grid properties may underlie the coding of distance.

2.3 Grid variability and distance coding in 2D

We extend our analysis to 2D environments. This introduces two changes to our numerical simulations. First, unlike 1D environments where grid cells can be locked to the starting location [22], in 2D environments grid cells are found to have distributed grid phase [1]. Therefore, for each noisy synthetic grid cell we simulate, we sample its grid phase from a uniform distribution over all possible translations. And second, we remove the assumption that the grid orientation is set to $0°$. Therefore, we consider the existence of non-zero variability in grid orientation ($\sigma_\theta > 0°$). In addition, when simulating grid cells coming from multiple modules, we assume that each module has its own orientation [2].

As in the 1D environment, we find that a single grid module, with a fixed grid spacing and orientation, does not show any distance dependent correlation with the population vector at the center of the environment, $(x, y) = (0, 0)$ (Fig. 5A). Similarly, we find that populations of grid cells coming from three modules with fixed grid properties exhibit a non-monotonic relationship between distance and correlation (Fig. 5B). However, grid cells from a single grid module with heterogeneity in grid properties has a monotonic decay of correlation, as a function of distance (Fig. 5C). While the relationship is similar to the 1D case (where $\sigma_\theta = 0°$ and there is no distribution of grid phase – Fig. 2F), there is an important difference. In particular, the asymptotic correlation value is ≈ 0.6, instead of ≈ 0.8. This implies that there is greater de-correlation in 2D environments, with σ_θ acting to further separate population vectors. This can be seen clearly when we fix the λ, θ, and σ_λ, and vary σ_θ. In particular, we find greater de-correlation with increasing grid orientation variability (Fig. 5D). In addition, we find that greater σ_θ leads to faster de-correlation (Fig. 5D), as was found with increasing grid spacing variability in the 1D setting (Fig. 2H).

By shaping the distance dependence of the population vector correlation, σ_θ also shapes the trade-off between the distinguishability of different locations and the distance over which the de-correlation occurs. In particular, for a given λ and θ, we find that increasing either σ_λ or σ_θ leads to an increase in maximum DoC (Fig. 5E), while at the same time leading to a rapid decrease in location of maximum DoC (Fig. 5F). Interestingly, we find that $\sigma_\theta = 0.5°$ and $\sigma_\lambda = 0.02$ m, which was the average variability found across all experimentally recorded modules previously analyzed [16], achieves both an intermediate value of maximum DoC and maximum DoC location (Fig. 5E, F). This suggests that grid property variability may be tuned to enable accurate of distance coding, over non-trivial ranges.

3 Discussion

The organization of grid cells into discrete modules [2] has led many theoretical investigations on their computational role to make the corollary assumption that, within a module, all grid cells are identical, up to translation [14, 17–19, 25]. While experimental investigation has found evidence that grid cells are involved in the computing of distance between points [8–10], the assumption of a single grid spacing and orientation, per grid module, has required complex coding schemes to achieve this for distances > 1.0 m [3].

Recent analysis of state-of-the-art electrophysiological recordings of medial entorhinal cortex [26] identified small, but robust heterogeneity in grid properties within the same grid module [16]. This variability leads to a breaking of the grid cell population activity translation symmetry, and suggests that individual grid modules may have considerably more computational capacity than was previously assumed.

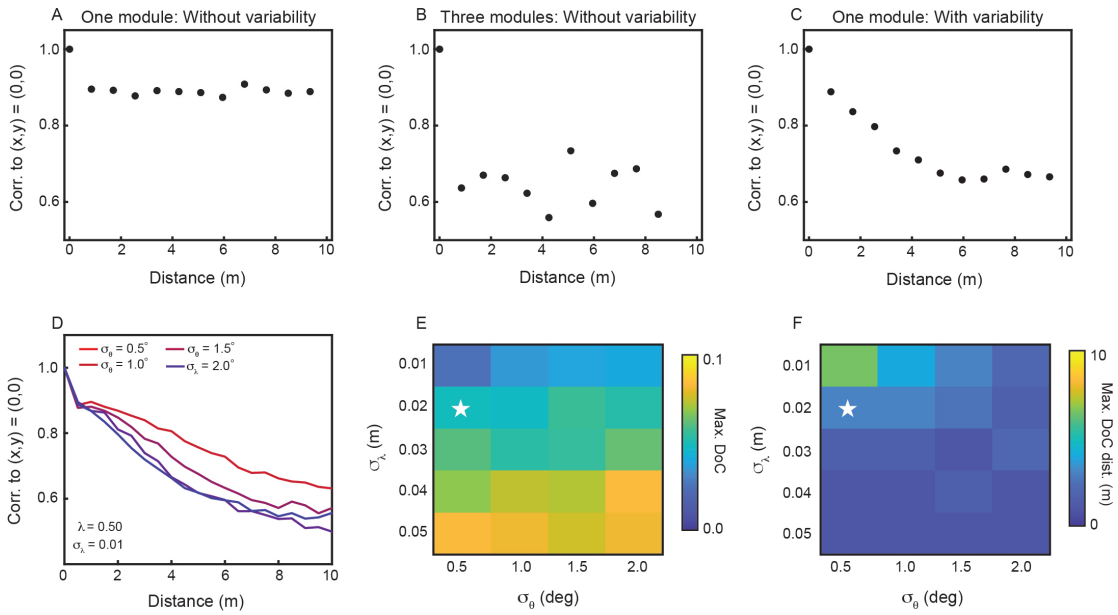

Figure 5: **Variability in grid properties leads to monotonic relationship between population vector correlation and distance in 2D.** (A)–(C) Correlation of population vectors, corresponding to distances at integer multiples of grid spacing along the x–axis, with the population vector corresponding to the center of the 2D arena, for different populations of grid cells. (D) Population vector correlation, as a function of distance, for different grid orientation variabilities, σ_θ. λ is fixed at 0.50 m and σ_λ is fixed at 0.01 m. (E) Maximum DoC value for different combinations of σ_λ and σ_θ. (F) Distance at which the maximum DoC value was achieved, for different combinations of σ_λ and σ_θ. (E)–(F) White star denotes previously found value of σ_λ and σ_θ in analysis of experimentally recorded grid cells [16]. For all plots, $\theta = 0°$, $N = 128$, and 25 unique populations were simulated.

In this work, we hypothesize that heterogeneity of grid properties, within a grid module, generates distance dependent de-correlation of population activity (Fig. 1), enabling simple decoding of distance. We develop a theory for the effect heterogeneity in grid spacing has on population vector correlation, as a function of distance, in one-dimension, which predicts a trade-off between the range over which the de-correlation occurs (maximized by increasing λ or decreasing σ_λ) and the distinguishability between different locations (maximized by decreasing λ or increasing σ_λ). Numerical simulations support the presence of such a trade-off in both 1D (Fig. 2) and 2D (Fig. 5), where variability in grid orientation further influences how the de-correlation occurs. These results provide new insight on why the observed range of grid properties, within a given module, is relatively limited. In particular, optimally encoding distance requires balancing both range and distinguishability, pushing the optimal σ_λ and σ_θ towards small (but not too small) values. Such small variability is not optimal for encoding local spatial position, the previously suggested role for grid heterogeneity [16], as increasing variability only improves accuracy.

Importantly, we find that decoding distance from de-correlation is not easily viable when considering grid cell activity from multiple modules. This is due to the quasi-periodic relationship in grid spacing between grid modules [2], leading to a non-monotonic relationship between population vector correlation and distance (Fig. 2). This lack of order becomes increasingly clear when considering grid cells in 2D, as the grid orientation of each module is independent and not generally aligned [2]. Thus, unlike local spatial coding – where considering activity of grid cells from multiple grid modules improves the fidelity of the code [3, 16–19] – distance coding is particularly enabled when considering activity only from a single grid module with non-zero grid property variability.

Our simulations led us to identify that a distance by de-correlation code has a "sweet spot", at which distance is well encoded (Fig. 3). We find evidence for this in previously published rodent behavioral experiments [10], and find that a decoding of distance from the population vector correlation of noisy synthetic grid cells generates results that are consistent with these experiments (Fig. 4). This is a non-trivial

prediction, as distortions to the periodic order of grid cells [27, 28], through the presence of sheering or compression, would be expected to lead only to an increase in distance coding error.

Limitations. The distance by de-correlation code we study enables coding of distance only at integer multiples of the grid spacing. While this can provide information that is behaviorally relevant (e.g., is the nest near-by, < 1 m, or far away, > 5 m), it does not provide finer-scale distance information. In addition, how such a code can be reliably readout in a biologically plausible manner remains to be studied, particularly in two-dimensional environments, where movement along the axes of the grid is necessary. However, we note that in some cases, there may be an obvious spacing that may be most natural to compute distance with respect to (e.g., distance between aisles in a grocery store). This can also be true in "abstract" spaces, where grid cells have been known to emerge [29, 30]. For instance, in recent work where non-human primates "traveled" between different images, there was a set spacing between each image [31], providing a natural reference distance.

The theory we develop assumes no noise. This limits its applicability to real grid cell recordings, where grid cell firing fields often exhibit significant departure from pure Gaussians. However, we find that simulating synthetic populations of grid cells, modeled as Poisson processes, generate results that are consistent with the theory. This suggests it is capable of providing insight that is relevant even in the more realistic setting.

Finally, while our decoding analysis provides results that are broadly consistent with Tennant et al.'s (2018) experiments, there is an important difference. Decoding using the population vector correlation leads to an increase in error at a distance equal to twice the grid spacing (1.6 m) (Fig. 2C). This contrasts the experimental finding that accuracy stays high up to approximately 1.5 m (Fig. 2B). In addition, the behavioral experiments were only performed with at most 7 mice [10]. Therefore, it remains to be seen whether the sweet spot is due to the specifics of the experiment or is instead a more general property. This can be tested in future experiments.

Future directions. While detailed analysis has shown the presence of robust within module grid property variability [16], broader characterization of such heterogeneity remains to be done. Performing this analysis on more datasets, across different model species (e.g., mouse, rat, bat) will not only increase our understanding of the prevalence of grid heterogeneity, but will also provide greater understanding of how the trade-off between the range over which de-correlation occurs and the distinguishability between distances is balanced.

Computational advantages of having grid cells with variable properties within a single grid module, beyond distance coding, may exist. Indeed, it is well appreciated in the computational neuroscience community that heterogeneity in neuron responses can be useful for increasing robustness [32–34]. Future work should explore whether other uses of grid heterogeneity exist. In addition, how the heterogeneity arises, and how it is maintained by a 2D attractor network, remains an outstanding open question that should be addressed.

Acknowledgments

We thank Michael Goard, Santiago Acosta-Mendoza, and Xue-Xin Wei for helpful discussions on the role of grid property heterogeneity. P. D. is supported by the INSPIRE scholarship from the Department of Science and Technology (DST), under the Ministry of Science and Technology, Government of India. A.S.D.'s research is supported by the EPSRC Centre for Doctoral Training in Mathematics of Random Systems: Analysis, Modelling and Simulation (EP/S023925/1). A.S.D.'s research is also funded by the President's PhD Scholarships at Imperial College London. A.S.D. would also like to acknowledge financial support from the NSF AI Institute for Artificial Intelligence and Fundamental Interactions, USA.

References

[1] Torkel Hafting, Marianne Fyhn, Sturla Molden, May-Britt Moser, and Edvard I Moser. Microstructure of a spatial map in the entorhinal cortex. *Nature*, 436(7052):801–806, 2005.

[2] Hanne Stensola, Tor Stensola, Trygve Solstad, Kristian Frøland, May-Britt Moser, and Edvard I Moser. The entorhinal grid map is discretized. *Nature*, 492(7427):72–78, 2012.

[3] Ila R Fiete, Yoram Burak, and Ted Brookings. What grid cells convey about rat location. *Journal of Neuroscience*, 28(27):6858–6871, 2008.

[4] Vemund Sigmundson Schøyen, Kosio Beshkov, Markus Borud Pettersen, Erik Hermansen, Konstantin Holzhausen, Anders Malthe-Sørenssen, Marianne Fyhn, and Mikkel Elle Lepperød. Hexagons all the way down: Grid cells as a conformal isometric map of space. *PLOS Computational Biology*, 21(2):e1012804, 2025.

[5] Dehong Xu, Ruiqi Gao, Wenhao Zhang, Xue-Xin Wei, and Ying Nian Wu. On conformal isometry of grid cells: Learning distance-preserving position embedding. In *The Thirteenth International Conference on Learning Representations*, 2025.

[6] Daniel Bush, Caswell Barry, Daniel Manson, and Neil Burgess. Using grid cells for navigation. *Neuron*, 87(3):507–520, 2015.

[7] Vegard Edvardsen, Andrej Bicanski, and Neil Burgess. Navigating with grid and place cells in cluttered environments. *Hippocampus*, 30(3):220–232, 2020.

[8] Stephen Duncan, Maneesh V Kuruvilla, Benjamin Thompson, Daniel Bush, and James A Ainge. Grid cell distortion is associated with increased distance estimation error in polarized environments. *Current Biology*, 2025.

[9] Pierre-Yves Jacob, Marta Gordillo-Salas, Justine Facchini, Bruno Poucet, Etienne Save, and Francesca Sargolini. Medial entorhinal cortex and medial septum contribute to self-motion-based linear distance estimation. *Brain Structure and Function*, 222(6):2727–2742, 2017.

[10] Sarah A Tennant, Lukas Fischer, Derek LF Garden, Klára Zsófia Gerlei, Cristina Martinez-Gonzalez, Christina McClure, Emma R Wood, and Matthew F Nolan. Stellate cells in the medial entorhinal cortex are required for spatial learning. *Cell reports*, 22(5):1313–1324, 2018.

[11] Vemund Sigmundson Schoyen, Kosio Beshkov, Markus Borud Pettersen, Erik Hermansen, Konstantin Holzhausen, Anders Malthe-Sorenssen, Marianne Fyhn, and Mikkel Elle Lepperod. Hexagons all the way down: Grid cells as a conformal isometric map of space. *bioRxiv*, pages 2024–02, 2024.

[12] Rishidev Chaudhuri, Yicong Zheng, Randall C O'Reilly, and Charan Ranganath. Not a global map, but a local hash: grid cells decorrelate the representation of position and scramble long-range distance information. *bioRxiv*, pages 2025–09, 2025.

[13] Dehong Xu, Ruiqi Gao, Wenhao Zhang, Xue-Xin Wei, and Ying Nian Wu. Conformal isometry of lie group representation in recurrent network of grid cells. In *NeurIPS 2022 Workshop on Symmetry and Geometry in Neural Representations*, 2022.

[14] Sameet Sreenivasan and Ila Fiete. Grid cells generate an analog error-correcting code for singularly precise neural computation. *Nature neuroscience*, 14(10):1330–1337, 2011.

[15] NM Van Strien, NLM Cappaert, and MP Witter. The anatomy of memory: an interactive overview of the parahippocampal–hippocampal network. *Nature reviews neuroscience*, 10(4):272–282, 2009.

[16] William T Redman, Santiago Acosta-Mendoza, Xue-Xin Wei, and Michael J Goard. Robust variability of grid cell properties within individual grid modules enhances encoding of local space. *bioRxiv*, pages 2024–02, 2024.

[17] Alexander Mathis, Andreas VM Herz, and Martin Stemmler. Optimal population codes for space: grid cells outperform place cells. *Neural computation*, 24(9):2280–2317, 2012.

[18] Xue-Xin Wei, Jason Prentice, and Vijay Balasubramanian. A principle of economy predicts the functional architecture of grid cells. *Elife*, 4:e08362, 2015.

[19] Martin Stemmler, Alexander Mathis, and Andreas VM Herz. Connecting multiple spatial scales to decode the population activity of grid cells. *Science Advances*, 1(11):e1500816, 2015.

[20] Revekka Ismakov, Omri Barak, Kate Jeffery, and Dori Derdikman. Grid cells encode local positional information. *Current Biology*, 27(15):2337–2343, 2017.

[21] Fabio Stefanini, Lyudmila Kushnir, Jessica C Jimenez, Joshua H Jennings, Nicholas I Woods, Garret D Stuber, Mazen A Kheirbek, René Hen, and Stefano Fusi. A distributed neural code in the dentate gyrus and in ca1. *Neuron*, 107(4):703–716, 2020.

[22] Malcolm G Campbell, Alexander Attinger, Samuel A Ocko, Surya Ganguli, and Lisa M Giocomo. Distance-tuned neurons drive specialized path integration calculations in medial entorhinal cortex. *Cell reports*, 36(10), 2021.

[23] Dennis W Ricker. *Echo Signal Processing*. The Springer International Series in Engineering and Computer Science. Springer, New York, NY, 2003 edition, February 2003.

[24] Trygve Solstad, Edvard I Moser, and Gaute T Einevoll. From grid cells to place cells: a mathematical model. *Hippocampus*, 16(12):1026–1031, 2006.

[25] Will Dorrell, Peter E. Latham, Timothy E. J. Behrens, and James C. R. Whittington. Actionable neural representations: Grid cells from minimal constraints. In *The Eleventh International Conference on Learning Representations*, 2023.

[26] Richard J Gardner, Erik Hermansen, Marius Pachitariu, Yoram Burak, Nils A Baas, Benjamin A Dunn, May-Britt Moser, and Edvard I Moser. Toroidal topology of population activity in grid cells. *Nature*, 602(7895):123–128, 2022.

[27] Julija Krupic, Marius Bauza, Stephen Burton, Caswell Barry, and John O'Keefe. Grid cell symmetry is shaped by environmental geometry. *Nature*, 518(7538):232–235, 2015.

[28] Gily Ginosar, Johnatan Aljadeff, Liora Las, Dori Derdikman, and Nachum Ulanovsky. Are grid cells used for navigation? on local metrics, subjective spaces, and black holes. *Neuron*, 111(12):1858–1875, 2023.

[29] Alexandra O Constantinescu, Jill X O'Reilly, and Timothy EJ Behrens. Organizing conceptual knowledge in humans with a gridlike code. *Science*, 352(6292):1464–1468, 2016.

[30] Dmitriy Aronov, Rhino Nevers, and David W Tank. Mapping of a non-spatial dimension by the hippocampal–entorhinal circuit. *Nature*, 543(7647):719–722, 2017.

[31] Sujaya Neupane, Ila Fiete, and Mehrdad Jazayeri. Mental navigation in the primate entorhinal cortex. *Nature*, 630(8017):704–711, 2024.

[32] Maoz Shamir and Haim Sompolinsky. Implications of neuronal diversity on population coding. *Neural computation*, 18(8):1951–1986, 2006.

[33] Mircea I Chelaru and Valentin Dragoi. Efficient coding in heterogeneous neuronal populations. *Proceedings of the National Academy of Sciences*, 105(42):16344–16349, 2008.

[34] Nicolas Perez-Nieves, Vincent CH Leung, Pier Luigi Dragotti, and Dan FM Goodman. Neural heterogeneity promotes robust learning. *Nature communications*, 12(1):5791, 2021.

A Synthetic grid cell simulations

We simulate synthetic populations of noisy grid cells following the same approach used by Redman et al. (2025). We provide a summary below.

An environment of size $L_x \times L_y$ defines the space over which the grid cell patterns exist. In the case of 1D experiments, $L_y = 0$ m. Then, for $N \in \mathbb{N}$ grid cells, the grid spacing and orientation of each grid cell is sampled via $\lambda_i \sim \mathcal{N}(\lambda, \sigma_\lambda^2)$ and $\theta_i \sim \mathcal{N}(\theta, \sigma_\theta^2)$, where $\mathcal{N}(\mu, \sigma^2)$ is a normal distribution with mean μ and variance σ^2. Grid phase is sampled as $\phi_i \sim \mathcal{U}([0, L_x] \times [0, L_y])$, where ϕ is a two dimensional vector, with first component uniformly sampled from $[0, L_x]$ and second component uniformly sampled from $[0, L_y]$. To construct a population with no variability in grid properties, we set $\sigma_\lambda = 0$ m and $\sigma_\theta = 0°$. As noted in the main text, when simulating a 1D environment, $\phi_i = 0$ m and $\theta_i = 0°$, for all N grid cells.

For each grid cell, we generate an idealized grid response by summing three two-dimensional sinusoids [24], such that the activity at $\mathbf{x} = (x, y) \in [-L_x/2, L_x/2] \times [-L_y/2, L_y/2]$ is given by

$$G^{(i)}_{\lambda_i,\theta_i,\phi_i}(\mathbf{x}) = X^{\max}\frac{2}{3}\left(\frac{1}{3}\sum_{j=1}^{3}\cos\left[\mathbf{k}_j(\theta_i)(\mathbf{x}+\phi_i)\right] + \frac{1}{2}\right), \tag{15}$$

where $X^{\max}$ is the maximal firing rate and $\mathbf{k}_j(\theta_i)$ are the wave vectors with 0°, 60°, and 120° angular differences

$$\begin{aligned}
k_1(\theta_i) &= \frac{k}{\sqrt{2}} \cdot [\cos(\theta_i + \pi/12) + \sin(\theta_i + \pi/12), \cos(\theta_i + \pi/12) - \sin(\theta_i + \pi/12)] \\
k_2(\theta_i) &= \frac{k}{\sqrt{2}} \cdot [\cos(\theta_i + 5\pi/12) + \sin(\theta_i + 5\pi/12), \cos(\theta_i + 5\pi/12) - \sin(\theta_i + 5\pi/12)] \\
k_3(\theta_i) &= \frac{k}{\sqrt{2}} \cdot [\cos(\theta_i + 3\pi/4) + \sin(\theta_i + 3\pi/4), \cos(\theta_i + 3\pi/4) - \sin(\theta_i + 3\pi/4)],
\end{aligned} \tag{16}$$

where $k = 4\pi/(\sqrt{3}\lambda_i)$.

We generated noisy spike rates of N grid cells by assuming a Poisson process and sampling using the idealized ratemaps (Eq. 15). More concretely, the activity of grid cell i at position $\mathbf{x} = (x, y)$ was assumed to be a random variable with a Poisson distribution, whose mean was $G^{(i)}_{\lambda_i,\theta_i,\phi_i}(\mathbf{x})$. Thus, the probability of observing $\tilde{G}^{(i)}_{\lambda_i,\theta_i,\phi_i}(\mathbf{x})$ spikes is given by

$$\tilde{G}^{(i)}_{\lambda_i,\theta_i,\phi_i}(\mathbf{x}) \sim \mathcal{P}\left[G^{(i)}_{\lambda_i,\theta_i,\phi_i}(\mathbf{x})\right]. \tag{17}$$

For all numerical experiments, we set $X^{\max} = 15$.

B Decoding analysis

Inspired by the rodent behavioral experiment results from Tennant et al. (2018), showing a "sweet spot" in distance coding, we performed a decoding analysis on populations of simulated noisy grid cells (Appendix A). In particular, we sought to explore the kinds of error patterns that emerge when decoding distance from grid cells with heterogeneous grid properties, and to compare these error patterns to those found in the behavioral data.

We consider a 1D environment of length 10 m (i.e., $L_x = 10$ m) and a population of N grid cells, whose grid spacing is sampled as $\lambda_i \sim \mathcal{N}(\lambda, \sigma_\lambda^2)$. We then generated M different realizations of the Poisson process, $\tilde{G}^{(i)}_{\lambda_i}(x)$. This gives $\tilde{G}^{(i,j)}_{\lambda_i}(x)$, where $j = 1, ..., M$. That is, we have M noisy population vectors, $\tilde{\mathbf{G}}^{(j)}_{\lambda}(x)$, for each location in space along the 1D environment. For each of the M population vectors, we compute the correlation function, $C^{(j)}(x)$, which measures the correlation between $\tilde{\mathbf{G}}^{(j)}_{\lambda}(x)$ and $\tilde{\mathbf{G}}^{(j)}_{\lambda}(0)$, where $x = n\lambda$, $n \in \mathbb{N}$.

We perform cross-validated distance decoding using the correlation functions. That is, we average $M - 1$ of the correlation functions and then use that as a template to decode location based on the remaining correlation function. More precisely, we compute the average correlation function, $\widehat{C}(x) = 1/(M-1)\sum_{m=1}^{M-1} C^{(m)}(x)$. Then, for a given integer multiple of the grid spacing $n\lambda$, we assign its decoded location to be

$$\tilde{x} = \min\left\{x \;\middle|\; \left|\frac{C^{(M)}(n\lambda)}{\widehat{C}(x)} - 1\right| < \tau\right\}. \tag{18}$$

Assigning the minimum distance where the observed value of $C^{(M)}(n\lambda)$ is within τ percent of the average correlation, $\widehat{C}(x)$, is inspired by the fact that the rodents in the behavioral experiments tended to stop before the reward zone. This suggests that they stop once evidence has reached a certain threshold.

In the above description, we have – for simplicity – used the first $M-1$ realizations of the population vector as the "train" set and the last correlation vector as the "test" set. In practice, we repeated this process M times, each realization being used once as the test set. We take the average error across all M decoded values. We repeat this whole process K times, to sample different populations of grid cells.

For our numerical experiments, we set $M = 10$, $\tau = 0.05$, $K = 7$, and $N = 64$.